Case Study: Vertical Drain and Stability Analyses for a Compacted Embankment on Soft Soils

Timothy D. Stark, Ph.D., P.E., D.GE, F.ASCE[1]; Perry J. Ricciardi, P.E., A.M.ASCE[2]; and Ryan D. Sisk, A.M.ASCE[3]

Abstract: This case study describes the failure of an interstate connecting-ramp embankment during construction and investigates the failure mechanism, performance of the prefabricated vertical drains (PVDs) installed to accelerate consolidation of the weak embankment foundation soils, embankment shear strength parameters, and design slope stability analyses. The weak, fine-grained foundation soil experienced less drainage, and thus less consolidation and strength gain, than expected via the PVDs because of an overestimate of the design horizontal coefficient of consolidation. As a result, the inverse analyses show the failure was caused by lower than expected shear strength of the foundation soils and an overestimate of the compacted embankment shear strength. The compacted embankment fill strength was characterized using an undrained shear strength, i.e., cohesion, without a tension crack, which inflated the calculated factor of safety. Recommendations to estimate embankment shear strength parameters, depth of embankment tension crack, bearing capacity factor of safety for comparison with limit equilibrium values, and horizontal consolidation properties for PVD design for future embankment projects are presented. **DOI: 10.1061/(ASCE)GT.1943-5606.0001786.**

Author keywords: Shear strength; Slope stability; Consolidation; Compacted fill; Prefabricated vertical drains; Bearing capacity analysis; Coefficient of horizontal consolidation.

Introduction

This paper presents a case study analyzing the failure of a 91-m-long (300-ft) section of a connecting-ramp embankment (Ramp ES) between westbound Interstate-76 (I-76) and southbound Interstate-71 (I-71) in Medina County, Ohio. The 91 m-long (300 ft) section between Stations 202+00 and 205+00 failed during construction at just over 43% of the design height (9.2 m; 30 ft). The widening and reconstruction of I-71 at the I-76 interchange included the addition of a third lane for 5.2 km (3.2 miles) of I-71, construction of new ramps and embankments, and demolition and reconstruction of 14 bridges. The plans and specifications for this project were completed in 2004.

An aerial view of the interchange, construction work in early 2007, and location of Ramp ES is presented in Fig. S1 in Appendix S1 for orientation and project scale. A key design feature of the Ramp ES design was the use of prefabricated vertical drains (PVDs) to accelerate consolidation and increase shear strength of the weak, fine-grained foundation soils under the connecting-ramp embankment. The design of the PVDs sought to increase the foundation soil shear strength by a factor of 2.0–2.5 to develop an adequate factor of safety during placement, which is discussed subsequently. However, after only 2.4 m (8 ft) of embankment fill placement, or just over one-quarter of the full embankment height of 9.2 m (30 ft) at this location, tension cracks began to appear along the crest of the embankment. After the embankment height reached approximately 43% (4.0 m; 13 ft) of the full height (9.2 m; 30 ft), a 91-m-long (300-ft) section of the embankment failed in 2007.

This embankment failure was unfortunate because ODOT decided to replace the embankment with a $4.5 million reinforced concrete bridge over the poor foundation soils associated with the Ramp ES failure instead of using a geotechnical-based solution, as discussed subsequently. This paper presents an evaluation of the failure mechanism, PVD design and performance, embankment shear strength parameters and tension crack, and slope stability and bearing capacity analyses to facilitate future highway embankment design and construction in Ohio.

Subsurface Conditions at Ramp ES

Soil Profile

A total of 100 test borings were completed for this project. Twenty-four of these 100 borings were completed along the 1,705.8 m-long (520.0 ft) Ramp ES, with 13 near the failure area (Fig. 1). The borings extended to depths between 4.6 and 22.9 m (15–75 ft) below ground surface. The soil profile generally consisted of a thin (~0.3 m; 1 ft) layer of topsoil overlying various layers of fine-grained soil. The fine-grained soils were brown and/or gray, mottled, clayey silt or silty clay with lesser percentages of sand and gravel. Very soft to soft silty clays, sandy silts, and organic clays ranging from depths of 0.3 to 11.6 m (1–38 ft) had organic contents ranging from 3 to 84% as determined by ignition tests [ASTM D2974-14 (ASTM 2014a)]. The majority of this material was classified as an organic clay, not peat, under ASTM D4427-13 (ASTM 2013a), because peat classification requires an organic content greater than 75% under ASTM D2974-14.

[1]Professor, Dept. of Civil and Environmental Engineering, Univ. of Illinois at Urbana-Champaign, 205 N. Mathews Ave., Urbana, IL 61801 (corresponding author). E-mail: tstark@Illinois.edu; tstark@uiuc.edu

[2]District #3 Testing Engineer, Ohio Dept. of Transportation, 906 Clark Ave., Ashland, OH 44805. E-mail: Perry.Ricciardi@dot.ohio.gov

[3]Staff Engineer, Terracon Consultants, Inc., 15080 A Circle, Omaha, NE 68144. E-mail: rdsisk2@terracon.com

Note. This manuscript was submitted on February 9, 2016; approved on May 25, 2017; published online on November 17, 2017. Discussion period open until April 17, 2018; separate discussions must be submitted for individual papers. This paper is part of the ***Journal of Geotechnical and Geoenvironmental Engineering***, © ASCE, ISSN 1090-0241.

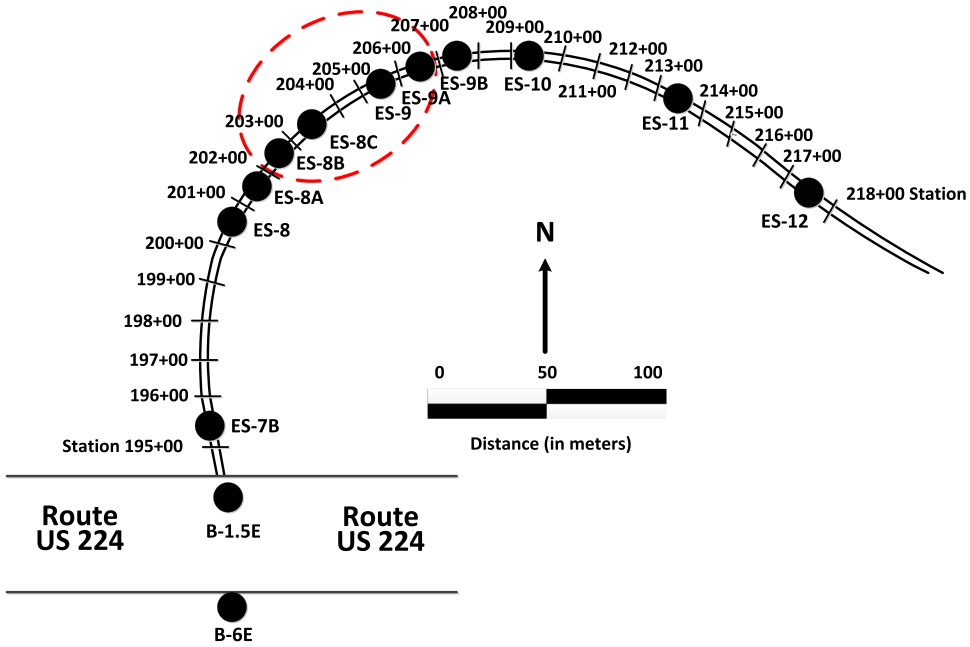

Fig. 1. Location of ES labelled borings along Ramp ES, with slope failure area marked by dashed circle

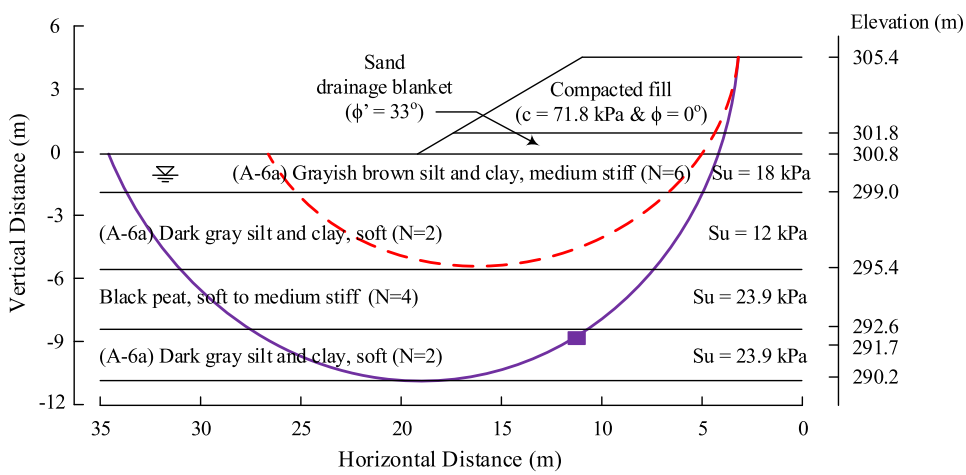

Fig. 2. Initial design cross section based on Boring ES-8A at Station 201+61, estimated undrained shear strengths, design critical failure surface (dashed circle), depth of movement at 15.2 m (50 ft) in slope inclinometer at Station 200+00 (solid block) at elevation +291.7 m, and observed failure surface (solid circle)

Groundwater was encountered in all but 6 of the 24 borings drilled along Ramp ES. Depths of the groundwater ranged from 0.4 to 7.5 m (1.3–24.0 ft), with the average depth being 3.2 m (10.5 ft). In almost all of the borings, cave-ins occurred after removal of the auger, which likely influenced the groundwater readings.

Some boring locations had 6.1 m (20 ft) or more of consecutive standard penetration test (SPT) blow counts (N) of 1 or W, indicating the weight of the hammer itself advanced the split spoon sampler 0.2 m (0.7 ft). A senior geotechnical engineer for the ODOT Office of Geotechnical Engineering (OGE) described the subsurface conditions within the interchange area as some of the most challenging the OGE had encountered, and the Ramp ES subsurface conditions were the worst on this project, with moisture contents at or above the liquid limit, as discussed subsequently.

Fig. 2 shows the initial design cross section at Station 201+61, which is based on Boring ES-8A and was just outside of the failure area (Fig. 1). The groundwater was found after drilling in Boring ES-8A at a depth of about 1 m (Fig. 2). This cross section was used to evaluate the stability of Ramp ES before and during construction by the designer and OGE. However, the Ramp ES slope failure occurred between Stations 202+00 and 205+00, so the subsurface conditions in the failure area were slightly different than the initial design cross section at Station 201+61. Fig. 3 shows the slightly different cross section for Station 203+58, which was closer to the center of the slide area, is based on Boring ES-8C (Fig. 1). The groundwater was found after drilling in Boring ES-8C at a depth of approximately 2 m (Fig. 3).

Soil Properties

Blow counts and pocket penetrometer readings were used to derive many of the soil properties for initial design, including unconfined

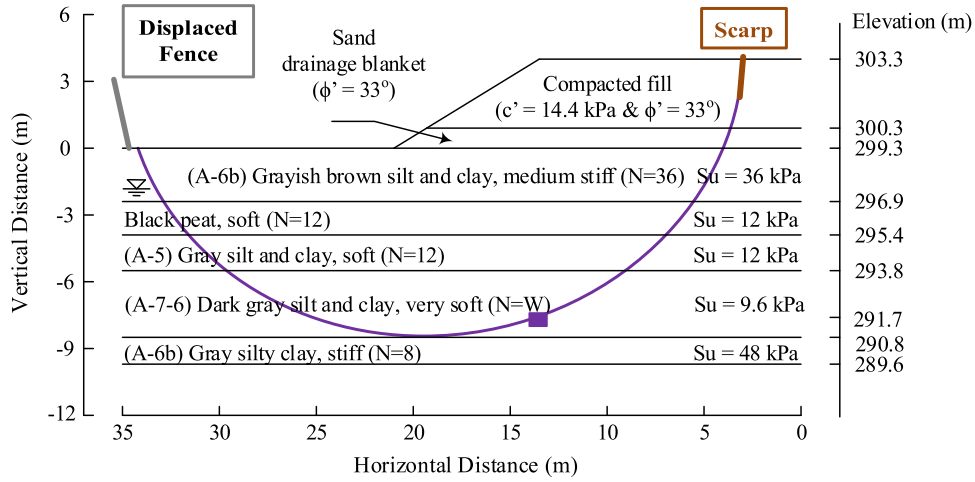

Fig. 3. Subsurface cross section for failed embankment based on Boring ES-8C at Station 203+58, estimated undrained shear strengths, depth of movement at 15.2 m (50 ft) in slope inclinometer at Station 200+00 (solid block) at Elevation +291.7 m, and observed failure surface (solid circle)

Table 1. Correlations between Soil Consistency, SPT Blow Count, and Unconfined Compressive Strength (q_u) from Bowles (1977) and Bowles (1996)

Soil	Bowles (1977)		Bowles (1996)	
Consistency	Blow count (N_{60})	q_u (kPa)	Blow count (N_{60})	q_u (kPa)
Very soft	0–2	<24	0–2	<25
Soft	3–4	24–48	3–5	25–50
Medium	4–8	48–96	6–9	50–100
Stiff	8–16	96–192	10–16	100–200
Very stiff	16–32	192–383	17–30	200–400
Hard	>32	>383	>30	>400

compressive strength (q_u), using empirical correlations and ODOT specifications (ODOT 1995).

Table 1 shows correlations between N and q_u from Bowles (1977, 1996) that were used before and during construction by the designer and OGE to evaluate embankment stability. The blowcount-based correlations in Bowles (1977, 1996) should be used with caution or avoided for clays. In fact, Peck et al. (1974) stated that the standard penetration based correlations "for clays can be regarded as no more than a crude approximation."

Soil samples from the 100 borings were preserved and visually classified in the laboratory in accordance with ASTM D2488-09 (ASTM 2009). Of these obtained samples, some were tested in the laboratory (see Table 2 for tests performed) to estimate the soil properties for the entire project. Even with this large number of borings and laboratory tests, an embankment failure occurred, which suggests improvements in the sampling, testing, analysis, and design phases are still needed.

Table 3 presents the index and engineering properties for the weak foundation soil A-6a at Station 201+61 of Ramp ES based on Boring ES-8A (Fig. 2) and used for the initial design. In Boring ES-8A, the initial moisture content was at or above the liquid limit, which is an indication, and a warning, of the low shear strength of the A-6a foundation soil. The boring log for borings ES-8A is included in Appendix S1 for completeness.

Table 4 presents the index and engineering properties for the weak foundation soil A-7-6 at Station 203+58 based on samples from Boring ES-8C (Fig. 3), which was in the failure area and used for the inverse analysis conducted herein. In Boring ES-8C, the initial moisture content was also at the liquid limit, which is an indication, and a warning, of the low shear strength of the A-7-6 foundation soil. The boring log for boring ES-8C is included in Appendix S2 for completeness.

Table 5 presents the unconfined compression strengths (q_u) from the 21 unconfined compression tests on samples obtained from Borings B-1.5E and B-6E at Stations 198+63 and 196+45, respectively, which were the closest borings with q_u data to Borings ES-8A and ES-8C. No unconfined compression tests were performed on samples from Boring ES-8A or Boring ES-8C. Borings B-1.5E and B-6E were drilled for the bridge over U.S. Route 224 (Fig. 1), which connects the two sides of Ramp ES across U.S. Route 224. As a result, these borings were not located at the slope

Table 2. Laboratory Testing Performed on Samples from the 100 Borings Drilled for the Entire Project

Laboratory test	ASTM test designation	Number of tests performed for entire project
Natural moisture content [ASTM D2216-10 (ASTM 2010b)]	ASTM D2216-13	1,277
Gradation—Hydrometer	ASTM D422-07 (ASTM 2007)	341
Gradation—Sieve	ASTM D422-07	50
Plastic and liquid limits	ASTM D4318-10 (ASTM 2010a)	347
Loss by ignition	ASTM D2974-14	82
Consolidation	ASTM D2435M-11 (ASTM 2011b)	5
Consolidated-undrained (CU) triaxial compression test series	ASTM D4767-11 (ASTM 2011a)	2
Unconfined compression tests	ASTM D2166-13 (ASTM 2013b)	21

Table 3. Measured Index and Engineering Properties of Soil A-6a (Gray Silt and Clay) from Samples SS-2, SS-5, and SS-12 from Boring ES-8A at Station 201+61 at Depths of 1.4, 3.7, and 10.4 m, Respectively

Parameter	Design value
Liquid limit (ASTM D4318-10)	33, 37, and 35
Plastic limit (ASTM D4318-10)	19, 24, and 22
Plasticity index (ASTM D4318-10)	14, 13, and 13
Initial moisture content (ASTM D2216-10) (%)	29, 44, and 49
Dry unit weight [kN/m^3 (pcf)]	12.5 kN/m^3 (79.4 pcf)
Total unit weight [kN/m^3 (pcf)]	17.3 kN/m^3 (110.1 pcf)
Initial void ratio (e)	1.36
Degree of saturation, S (%)	87.7
Specific gravity [ASTM D854-14 (ASTM 2014b)]	2.67
Preconsolidation pressure (kPa) Casagrande method (ASTM D2435)	150 kPa
Effective vertical stress (kPa)	77.6 kPa
Overconsolidation ratio (ASTM D2435)	1.9
C_v at 223 kPa (cm^2/min)	3.4×10^{-2} cm^2/min (1.78 m^2/year)
C_v at 418 kPa (cm^2/min)	4.70×10^{-2} cm^2/min (2.47 m^2/year)

Table 4. Measured Index and Engineering Properties of Soil A-7-6 (Mottled Gray Clay) from Sample SS-9 from Boring ES-8C at Station 203+58 at a Depth of 6.4 m

Parameter	Initial
Liquid limit (ASTM D4318-10)	45
Plastic limit (ASTM D4318-10)	23
Plasticity index (ASTM D4318-10)	22
Initial moisture content (%)	45.0
Dry unit weight [kN/m^3 (pcf)]	12.9 (82.4)
Total unit weight [kN/m^3 (pcf)]	18.1 (115.4)
Initial void ratio (e)	1.32
Degree of saturation, S (%)	92.3
Specific gravity (ASTM D854-14)	2.70

failure but were in close proximity. The boring logs for borings B-1.5E and B-6E are included in Appendixes S3 and S4, respectively, of the Supplemental Data for completeness.

The values of q_u ranged from 7.2 to 244.2 kPa with an average of 69.2 kPa (Table 5). This means the undrained shear strength, S_u, ranged from 3.6 to 122.1 kPa, with an average of 34.6 kPa. The average undrained shear strength ($0.5q_u$) for soil classifications A-6a, A-6b, A-7-5, A-7-6, and peat in Borings B-1.5E and B-6E from Table 5 were 35.2, 149.4, 46.9, 49.1, and 464.0 kPa, respectively. Two isotropically consolidated-undrained (CU) triaxial compression tests were conducted on samples ST-2 and ST-6 from Boring B-6E. The undrained shear strength parameters obtained from the CU triaxial compression tests on samples ST-2 and ST-6 were total stress: (1) cohesion values of 31.1 and 26.3 kPa, respectively; and (2) friction angles of 11.8° and 11.6°, respectively.

Table 6 presents the design slope stability input parameters for the subsurface cross section at Station 201+61 (Fig. 2) based on Boring ES-8A. Table 7 presents the slope stability input parameters for the subsurface cross section in the failure area at Station 203+58 (Fig. 3) based on Boring ES-8C and used for the inverse analyses conducted herein. The values of undrained shear strength in Tables 6 and 7 are significantly lower than the average undrained shear strength for soil classifications A-6a, A-6b, A-7-5, A-7-6, and peat based on the q_u values in Table 5, which are 35.2, 149.4, 46.9, 49.1, and 464.0 kPa, respectively. This helps explain why the slope failure did not occur near U.S. Route 224 where Borings B-1.5E and B-6 were drilled (Fig. 1).

Table 5. Measured Unconfined Compression Shear Strengths and Soil Types from Borings B-1.5E and B-6E at Stations 198+63 and 196+45, Respectively

Boring and sample number	Sample depth [m (ft)]	ODOT soil classification	Unconfined compressive strength [kPa (psf)]
B-1.5E, ST-1	1.4 (4.5)	A-6b	136.0 (2,840)
B-1.5E, ST-2	2.9 (9.5)	A-6a	41.2 (860)
B-1.5E, ST-3	4.4 (14.5)	A-6a	46.9 (980)
B-1.5E, ST-4	5.9 (19.5)	A-6a	17.2 (360)
B-1.5E, ST-5	7.5 (24.5)	A-7-5	49.8 (1,040)
B-1.5E, ST-6A	8.5 (28.0)	A-7-5	14.8 (310)
B-1.5E, ST-6B	8.8 (28.7)	Peat	170.4 (3,560)
B-1.5E, ST-7	10.1 (33.0)	Peat	1,555.5 (5,100)
B-1.5E, ST-8	11.7 (38.5)	Peat	97.2 (2,030)
B-1.5E, ST-9A	13.1 (43.0)	Peat	33.5 (700)
B-1.5E, ST-9B	13.3 (43.5)	A-7-5	54.6 (1,140)
B-1.5E, ST-10	14.6 (48.0)	A-6b	375.2 (1,230)
B-1.5E, ST-11	16.2 (53.0)	A-7-6	44.0 (920)
B-1.5E, ST-12	17.8 (58.5)	A-7-6	54.1 (1,130)
B-6E, ST-1	0.9 (3.0)	A-6b	165.2 (3,450)
B-6E, ST-3	4.0 (13.0)	A-6b	7.2 (150)
B-6E, ST-4C	5.8 (19.0)	A-7-5	57.5 (1,200)
B-6E, ST-5	7.0 (23.0)	A-7-5	25.8 (540)
B-6E, ST-7A	10.1 (33.0)	A-6a	20.6 (430)
B-6E, ST-7B	10.4 (34.0)	A-6a	50.3 (1,050)
B-6E, ST-8B	11.8 (38.8)	A-6b	63.2 (1,320)

To simulate the original embankment design, a singular value of undrained strength is used herein instead of estimating the undrained strength from an undrained strength ratio. As discussed subsequently, the increase in effective vertical stress, and thus shear strength, caused by consolidation due to the embankment fill is greatest at the embankment centerline and decreases toward the slope toe. As a result, the increase in shear strength due to consolidation along full length of the failure surface in Fig. 3 is probably small.

Undrained Shear Strength

Undrained shear strength, S_u, for stability analyses also can be interpreted from the relationship between S_u and preconsolidation pressure, σ'_p, instead of using blowcounts as was done for the initial design (Table 1). The ratio of S_u/σ'_p varies for the three shear modes along a circular failure surface due to changes in the effective major principal stress, σ'_{1f}. Eqs. (1)–(3) are based on empirical correlations between undrained strength ratio and plasticity index (PI) for these three modes of shear (Jamiolkowski et al. 1985; Terzaghi et al. 1996). However, these equations should be verified through laboratory or in situ testing before using them to estimate undrained shear strength for final design purposes (Terzaghi et al. 1996; Jamiolkowski et al. 1985; Holtz et al. 2011; Holtz and Kovacs 1981).

Triaxial compression is calculated as

$$\frac{S_u}{\sigma'_p} \sim 0.32 \quad \text{or} \quad \frac{S_u}{\sigma'_p} \sim 0.23 \pm 0.04(\text{OCR})^{0.8} \tag{1}$$

Table 6. Slope Stability Input Parameters for Subsurface Cross-Section at Station 201+61 Based on Boring ES-8A (Fig. 2)

Soil type	Total and saturated unit weights [kN/m^3 (pcf)]	Undrained shear strength (kPa/psf)	Effective and (ϕ') and total (ϕ) stress friction angles (degrees)
Compacted fill	21.2 (135)	71.8 (1,500)	$\phi' = 33$
Sand drainage blanket	18.6 (120)	0 (0)	$\phi' = 33$
(A-6a) gray/brown silt and clay	17.3 (110)	18.0 (375)	$\phi = 0$
(A-6a) dark gray silt and clay	17.3 (110)	12.0 (250)	$\phi = 0$
Black peat	11.8 (75)	23.9 (500)	$\phi = 0$
(A-6a) dark gray silt and clay	18.1 (115)	23.9 (500)	$\phi = 0$

Table 7. Slope Stability Input Parameters for Subsurface Cross-Section at Station 203+58 Based on Boring ES-8C (Fig. 3)

Soil type	Total and saturated unit weights [kN/m^3 (pcf)]	Undrained shear strength [kPa (psf)]	Effective and (ϕ') and total (ϕ) stress friction angles (degrees)
Compacted fill	21.2 (135)	71.8 (1,500) and 14.4 (300)	$\phi' = 33$
Sand drainage blanket	18.6 (120)	0	$\phi' = 33$
(A-6b) gray/brown silt and clay	17.3 (110)	36 (752)	$\phi = 0$
Black peat	11.8 (75)	12 (250)	$\phi = 0$
(A-5) gray silt and clay	17.3 (110)	12 (250)	$\phi = 0$
(A-7-6) dark gray silt and clay	15.7 (100)	9.6 (200)	$\phi = 0$
(A-6b) gray silty clay	18.1 (115)	48 (1,000)	$\phi = 0$

Direct simple shear is calculated as

$$\frac{S_u}{\sigma'_p} \sim 0.00061(\mathrm{PI}) + 0.22 \tag{2}$$

Triaxial extension is calculated as

$$\frac{S_u}{\sigma'_p} \sim 0.00117(\mathrm{PI}) + 0.13 \tag{3}$$

Alternatively, Terzaghi et al. (1996) showed that the mobilized undrained strength [$S_u(\mathrm{mob})$] along a circular failure surface, which is the case in Figs. 2 and 3, or a long gently inclined failure surface is

$$\frac{S_u}{\sigma'_p} = 0.22 \tag{4}$$

These equations show that the strongest mode of shear is compression, the weakest mode is extension, and the direct simple shear mode falls between those two modes of shear. When the effective vertical stress in a soil, σ'_v, is equal to or exceeds σ'_p, the ratio becomes equal to S_u/σ'_v. The value of σ'_v is determined from $\sigma'_v = \sigma'_{vo} + \Delta\sigma'_v$, where σ'_{vo} is the preconstruction in situ effective vertical stress and $\Delta\sigma'_v$ is the change in effective vertical stress from the surcharge load. Therefore as the foundation soil consolidates due to the PVDs, the undrained strength should increase. Table 3 presents the preconsolidation pressure for the weak foundation soil A-6a at Station 201+61 based on Boring ES-8A. Only five consolidation tests were performed for the entire initial design (Table 2), so more consolidation tests should be considered to better estimate the preconsolidation pressure for future projects if these empirical S_u/σ'_p relationships are used.

Ramp ES Design

The portion of Ramp ES that is the focus herein was designed on a new alignment traversing approximately 1,705.8 lineal m (5.593 lineal ft), a small stream, U.S. Route 224, County Road 97 (CR 97), and I-76 (Fig. S1). At its maximum height, the ramp was to be 9.8 m (32 ft) above the previous ground surface. In the area of the slope failure, the final embankment height is 9.2 m (30 ft). The bridges over I-76 and CR 97 are of conventional concrete design, but the permanent stream crossing was designed using a 3.7 × 3 m (12 × 10 ft) prefabricated box culvert under approximately 6 m (20 ft) of fill. The permanent culvert could not be installed until settlement of the foundation soils had occurred. Thus two 1.5-m-diameter (5-ft) corrugated metal pipes (CMPs) were installed temporarily to convey the stream flow during construction of the 9.2-m (30-ft) embankment, placement of an additional 3 m (10 ft) of surcharge, and the ensuing 6-month settlement period under the embankment and surcharge. After the 6-month settlement period, the 3-m (10-ft) surcharge would be removed to achieve the final embankment height of 9.2 m (30 ft). The surcharge fill was to be applied along the full length of Ramp ES and intended to achieve a greater preconsolidation pressure and undrained shear strength than that induced by the maximum final embankment height of 9.8 m (32 ft) to further increase embankment stability. Once embankment settlement was complete, the CMPs were to be removed so the permanent box culvert could be installed.

Piezometers were installed at various depths to monitor the pore-water pressures within the foundation soils during the consolidation process. A baseline pore-water pressure was established prior to embankment construction as discussed subsequently and the piezometers were read daily or after every new 0.3 m (1 ft) of embankment fill was placed to measure the change in pore-water pressure from this baseline. Six inclinometers were installed at Stations 196+00, 197+00, 198+00, and 200+00, which were not in the failure area between Stations 202+00 and 205+00, but these data are still discussed subsequently. The location, installation details, and data obtained from these slope inclinometers are shown in Appendix S6 of Supplemental Data for completeness.

The design of Ramp ES included a number of features to allow the weak foundation soils to consolidate and gain strength over time, e.g., PVDs and pore-water pressure monitoring, to achieve the desired long-term factors of safety for the embankment. Embankment fill placement could proceed until the measured pore-water

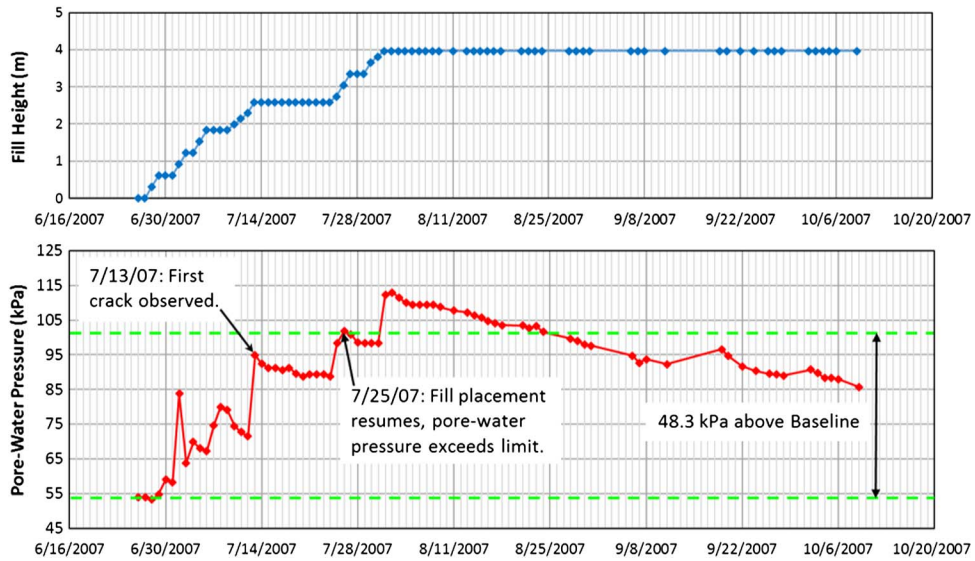

Fig. 4. Fill height, baseline pore-water pressure, and pore-water pressure versus time at Station 204+00 at elevation 295.7 m (Fig. 3)

pressures increased to 48.3 kPa (7 psi) above the baseline pore-water pressure of approximately 54 kPa (7.8 psi). If the change in pore-water pressure exceeded the baseline pressure plus 48.3 kPa (7 psi), i.e., approximately 102.0 kPa (14.8 psi), the fill placement would stop until the pore-water pressure decreased below 102.0 kPa (14.8 psi). The 48.3 kPa (7 psi) change in pore-water pressure was based on preliminary stability analyses and the ability of the PVDs to dissipate fill placement–induced pore-water pressures. Piezometer pore-water pressure and fill height controls mentioned previously were to be followed throughout Ramp ES embankment construction, as well as during construction of the 3-m (10-ft) surcharge fill on top of the embankment, for a total height of 12.2 m (40 ft).

Fig. 4 shows the as-built fill height and piezometer readings versus time at Station 204+00, which was in the slope failure area between Stations 202+00 to 205+00. As expected, the pore-water pressures steadily increased with increasing fill height. The cause of the sudden increase in pore-water pressure to 83.8 kPa on June 30, 2007 (Fig. 4) is not known. However, this isolated increase occurred early in the embankment filling and appears anomalous because the reading on the next day (July 1, 2007) was only 63.8 kPa, or approximately 20 kPa (25%) lower.

Ramp ES Construction from STA 202+00 to STA 205+00

A 0.9-m-thick (3-ft) sand drainage blanket was placed on the existing ground prior to PVD installation to facilitate drainage of water subsequently emerging from the PVDs due to consolidation (Fig. 3). The material used for the drainage blanket was a fine sand, and it was placed at a rate that did not exceed 0.3 m (1 ft) per day. The embankment fill material used for the construction of Ramp ES on top of the sand blanket came from mass excavation and pavement removal work on an I-71 project just north of the I-71/I-76 interchange. The embankment fill consisted of approximately 90% fine-grained soil and 10% broken concrete pavement and gravel base, based upon the initial geotechnical report, but additional concrete pieces were included, as discussed subsequently.

The PVDs, sand drainage blanket, and twin temporary CMP culverts for the stream crossing were installed in late fall of 2006. The piezometers, settlement monuments, and six inclinometers were installed in spring 2007. Placement of the first lift of fill at Ramp ES began on June 18, 2007. On July 13, 2007, when the embankment had reached only 2.4 m (8 ft), or just over one-quarter of the full embankment height (9.2 m or 30 ft) at this location, inspectors noticed tension cracks along the top of the embankment from Station 202+00 to Station 205+00 (Fig. 5). The tension cracks in Fig. 5 range in depth from 51 to 152 mm (2–6 in.). At that time, the foundation pore-water pressures had only increased 41 kPa (6 psi) above the 54 kPa (7.8 psi) baseline pore-water pressure, which was below the limiting increase of 48.3 kPa (7 psi) so construction could continue under the contract requirements.

The inclinometer at Station 200+00 was the closest to the failure area and showed a maximum cumulative displacement of approximately 50 mm at a depth of approximately 15.2 m (50 ft) beneath the top of the embankment fill (Fig. 2). A failure surface that corresponds to the tension cracks on the embankment crest, the inclinometer shear displacement at a depth of approximately 15.2 m (50 ft) at Station 200+00, and the observed toe of the slide mass, discussed subsequently, is shown in Fig. 2 and was deeper

Fig. 5. Initial tension cracks in Ramp ES embankment on July 13, 2007 (image courtesy of Ohio Department of Transportation)

Fig. 6. Cracking in Ramp ES embankment on October 15, 2007 after some erosion (image by Timothy D. Stark)

Fig. 7. Lateral movement of right-of-way fence near toe of Ramp ES embankment on October 15, 2007 (image by Timothy D. Stark)

than the design critical failure surface, which is also shown in Fig. 2. The inclinometer data were in agreement with the critical failure surface used in the postfailure analysis even though it was not located at Station 203+58 (Fig. 3). These inclinometer data reinforce the deeper critical failure surface identified in the postfailure analysis.

Between July 13, 2007 and July 24, 2007, embankment fill placement ceased while a geotechnical evaluation was completed by ODOT. On July 24, 2007, ODOT decided that embankment fill placement could resume but recommended that survey (PK) nails be installed along the embankment toe to monitor rotational movement. Between July 24, 2007 and August 1, 2007, the survey nails installed along the embankment toe showed uplift in the failure area, which was probably initial evidence of rotational movement.

By August 1, 2007, the embankment work reached a height of 4.0 m (13 ft). However, on August 1, 2007 additional tension cracks were noticed in the same location as the July 13, 2007 cracks along the embankment crest. Also on August 1, 2007, the pore-water pressure in the foundation soils exceeded 110 kPa (16 psi), which was 56.5 kPa (8.2 psi) above the baseline pressure (54 kPa; 7.8 psi), or 8.2 kPa (1.2 psi) above the allowable pore-water pressure increase of 48.3 kPa (7 psi).

On August 2, 2007, embankment construction was stopped and ODOT began reassessing the embankment stability and developing alternatives for the planned embankment construction. Between August 2, 2007 and August 6, 2007 embankment tension cracking along the crest progressed. Finally, on August 6, 2007, the northern half of the embankment rotated vertically downward 0.46 m (1.5 ft) and the foundation soils near the northern toe of the slope rose up. Fig. 6 shows the tension cracks along Ramp ES embankment on October 15, 2007 during a site visit by the first author. Fig. 6 also shows some of the broken concrete pavement pieces included in the fill material. Fig. 7 shows displacement of the nearby right-of-way fence on October 15, 2007, indicating that a deep-seated rotational foundation movement had occurred. Throughout embankment construction, there was little evidence of flow from the PVDs or the sand blanket. However, on August 6, 2007, water was observed draining from the sand blanket even though it had not been observed previously.

The Oregon Department of Transportation considered several options to reconstruct this portion of Ramp ES to control contract delay costs, which were estimated to be approximately $250,000 per month. The Oregon Department of Transportation considered reconstructing the embankment with lightweight fill, reinforcing the foundation soils with soil/concrete columns, and replacing the embankment with a bridge. The Oregon Department of Transportation eventually decided to replace the embankment with a $4.5 million reinforced concrete bridge extension of the planned bridge over U.S. 224. The originally planned 70-m-long (200-ft) reinforced concrete bridge over U.S. 224 was extended approximately 275 m (900 ft) across the poor foundation soil area of Ramp ES, including the stream. The Oregon Department of Transportation's decision was based on each of the embankment reconstruction options delaying the contract and relying on the weak foundation soils for support, which introduced significant risk. However, after construction of the 275-m-long (900-ft) bridge extension, the question remained of why the embankment failed even though the design indicated adequate stability. This question is the focus of this investigation, which presents an evaluation of the failure mechanism, PVD design and performance, embankment shear strength parameters and tension crack, and slope stability analyses to facilitate future highway embankment design and construction in Ohio.

Evaluation of Prefabricated Vertical Drain Performance

Consolidation of the weak foundation soils during embankment loading would require a significant amount of time because of the long vertical drainage path. As a result, one of the features of the Ramp ES design was the use of PVDs to accelerate primary consolidation of the weak fine-grained layers by reducing the drainage path and, in most cases, taking advantage of the larger coefficient of horizontal consolidation instead of the vertical coefficient (Mesri and Lo 1991; Lo 1991). The Ramp ES design utilized more than 99,060 m (325,000 ft) of PVDs installed on a 1.8-m (6-ft) equilateral triangle spacing, with an effective drainage area of approximately 2.9 m^2 (31 ft^2). The PVDs were 102 mm (4 in.) wide and 6 mm (0.25 in.) thick, with a discharge capacity through the core of at least 1.9 L/min (0.5 gal./min) measured under a normal stress of 239.4 kPa (5,000 psf) after a period of 24 h using a gradient of unity. The PVDs were installed with an anchor plate to keep the drain at or near the required depth when the T-shaped mandrel was removed during installation. The PVDs were installed to depths that fully penetrated the weak foundation layers and continued into the underlying firm soil.

J. Geotech. Geoenviron. Eng., 2018, 144(2): 05017007

Table 8. Projected Shear Strength Gain from Consolidation of Soft Foundation Soils and Resulting Embankment Factor of Safety

Fill height (m)			EOC 4.6 m	EOP 4.6 m	EOC 9.2 m	EOP 9.2 m
Depth (m)	Soil type	Design value	Undrained shear strength, S_u (kPa)			
0–2.4	A-6b	36.0	36.0	124.1	124.1	212.4
2.4–4	Peat	12.0	12.0	39.5	39.5	66.9
4–5.5	A-5	12.0	12.0	35.0	35.0	58.1
5–8.5	A-7-6	9.6	9.6	22.8	22.8	36.2
8.5–9.8	A-6b	48.0	48.0	100.5	100.5	153.1
Factor of safety		>1.3	0.88	1.80	1.04	1.48

Note: EOC = end of construction; EOP = end of primary consolidation.

Performance of PVDs

The performance of the PVDs installed in the embankment foundation was evaluated by estimating the strength gains and resulting FS that would result from 90% consolidation of the weak foundation soils. The strength gain from consolidation of the foundation soils was estimated from the undrained strength ratio and assuming an overconsolidation ratio (OCR) of unity, i.e., normally consolidated, so the effective vertical stress, σ_v', corresponds to the preconsolidation pressure.

The projected undrained shear strength after primary consolidation of the soft clay layers was calculated at different stages of construction using the S_u/σ_p' relationship equal to 0.22 and the increase in effective vertical stress from fill placement using a unit weight of 21.2 kN/m^3 (135 pcf). The increase in effective vertical stress used with S_u/σ_p' of 0.22 was based on the fill height at the centerline of the embankment (4.6 m at failure and 9.2 m at full height). The strength gain decreases from a maximum at the centerline to little or no increase at the slope toe. Table 8 shows the projected strength gain at the centerline and resulting FS at different stages of construction of the Ramp ES embankment. The projected strength gain after 90% consolidation should have produced a FS greater than or equal to 1.5 (Table 8) at staged construction heights of 4.6 and 9.2 m (15 and 30 ft). From the expected strength increase, it was concluded that embankment failure should not have occurred; thus the functionality of the PVDs is investigated herein.

Based on the measured pore-water pressures in Fig. 4, the PVDs probably did not produce the expected strength gain because of:

1. An overestimate of the horizontal coefficient of consolidation, i.e., horizontal hydraulic conductivity, of the foundation soils;
2. Filter cake formation on the filter geotextile surrounding the PVD that limited pore-water pressure dissipation;
3. Clogging of the PVD due to filter geotextile incompatibility with the foundation soils; and/or
4. Possible damage of the PVDs during installation, as discussed subsequently.

Consolidation of Weak Foundation Soils

The horizontal hydraulic conductivity is used to calculate the horizontal coefficient of consolidation, C_h, for PVD design; C_h is used to determine the degree of consolidation (U) at a given time as well as the overall time to reach the end of primary consolidation. The degree of consolidation, U, is computed from Terzaghi's theory of consolidation (Terzaghi et al. 1996) and the following equation:

$$U = 1 - \exp\left[\frac{-2T_r}{F_n}\right] \tag{5}$$

where $F_n = \ln(n) - 3/4$, $n = r_e/r_w$; r_e = radius of the soil cylinder discharging water into the PVD; r_w = equivalent radius of the PVDs; and T_r = time factor defined as

$$T_r = \frac{C_h t}{r_e^2} \tag{6}$$

where t = time.

Estimation of Mobilized Horizontal Coefficient of Consolidation

The value of C_h used to initially design the PVDs was 18.6 m^2/year (200 ft^2/year). This design value of C_h can be verified during fill placement and subsequent settlement using the Asaoka (1978) method to determine if consolidation and strength gain are occurring as expected and to facilitate use of the observational method described by Peck (1969). The C_h of the weak foundation soils was estimated herein using the Asaoka (1978) method, which uses field settlements with time to estimate the mobilized value of C_h (Asaoka 1978). The Asaoka method works by (1) selecting a series of measured settlements ($s_1, s_2, s_3, \ldots, s_j, s_{j+1}, \ldots$) corresponding to various times ($t_1, t_2, t_3, \ldots, t_j, t_{j+1}, \ldots$) but at a constant time interval, i.e., $t_{j+1} - t_j$ = constant; (2) plotting s_{j+1} against s_j; (3) drawing a straight line through the settlement versus time data; and (4) extrapolating the line to intersect a 45° line through the origin (Mesri and Huvaj-Sarihan 2009).

Urzua et al. (2016) showed that the Asaoka (1978) method yields good estimates of the mobilized C_h when PVDs are used and horizontal drainage controls the consolidation process. When vertical drainage controls the consolidation process, the Asaoka (1978) method yields reasonable values of mobilized vertical coefficient of consolidation, C_v, and settlement when the degree of consolidation is greater than 50% (Urzua et al. 2016). However, if the degree of consolidation is less than or equal to 50% and vertical drainage controls the consolidation process, the Asaoka (1978) method yields unsafe (too high) values of C_v, and another analysis method should be utilized (Urzua et al. 2016).

Table 9 presents the settlement data over time at Station 204+00 that were used to estimate the mobilized value of C_h in Table 10 using the procedure in Asaoka (1978). The point of intersection between the 45° line and the settlement data defines the EOP settlement, and the slope of the line is used to estimate the mobilized C_h. For one-dimensional compression with PVDs, C_h is calculated using

Table 9. Field Settlement Data over Time at Station 204+00 (Fig. 1)

Date	Settlement [m (ft)] $S(j)$	Settlement [m (ft)] $S(j+1)$
June 6, 2007	0	0
June 27, 2007	0.015 (0.05)	0
July 9, 2007	0.159 (0.52)	0
July 17, 2007	0.281 (0.92)	0
July 24, 2007	0.287 (0.94)	0.476 (1.56)
August 1, 2007	0.476 (1.56)	0.570 (1.87)
August 8, 2007	0.570 (1.87)	0.625 (2.05)
August 15, 2007	0.625 (2.05)	0.705 (2.31)
August 28, 2007	0.705 (2.31)	0.750 (2.46)
September 12, 2007	0.781 (2.56)	0.781 (2.7)
September 19, 2007	0.824 (2.70)	0.824 (2.86)
September 29, 2007	0.872 (2.86)	N/A

J. Geotech. Geoenviron. Eng., 2018, 144(2): 05017007

Table 10. Values of Mobilized Horizontal Coefficient of Consolidation Estimated using Asaoka (1978) Method

Station	Mobilized C_h (m^2/year)
202+00	7.7
203+00	8.4
204+00	6.4
205+00	19.0

$$C_h = \frac{\frac{-r_e^2}{E}\ln\beta}{\Delta t} \tag{7}$$

where β = slope of the line; Δt = constant time interval; and $E = 2/F(n)$, where $F(n)$ is a function of the maximum r_e, hydraulic conductivity of the soil (k_h), and drain smear zone (k_s), and radius of the smear zone (r_s)

$$F(n) = \frac{n^2}{n^2-1}\left(\ln\frac{n}{s} + \frac{k_h}{k_s}\ln s - \frac{3}{4}\right) + \frac{s^2}{n^2-1}\left(1 - \frac{s^2}{4n^2}\right) + \frac{k_h}{k_s}\frac{1}{n^2-1}\left(\frac{s^4-1}{4n^2} - s^2 + 1\right) \tag{8}$$

$$n = \frac{r_e}{r_w}$$
$$s = \frac{r_s}{r_w} \tag{9}$$

Fig. 8 shows the Asaoka (1978) plot of s_{j+1} against s_j for Station 204+00. The C_h values in Table 10 for Stations 202+00 to 204+00 (6.4–8.4 m^2/year) are well below the value of 18.6 m^2/year (200 ft^2/year) used in the initial design. Station 204+00, the center of the slope failure, produced the lowest value of mobilized C_h, i.e., 6.4 m^2/year (68.6 ft^2/year). This provides an explanation for the foundation soils not gaining sufficient undrained shear strength to maintain embankment stability. If the Asaoka (1978) method is used during construction and it is determined that the consolidation and strength gain is not occurring as anticipated, the filling process can be modified to maintain embankment stability, which is in agreement with the observational method (Peck 1969).

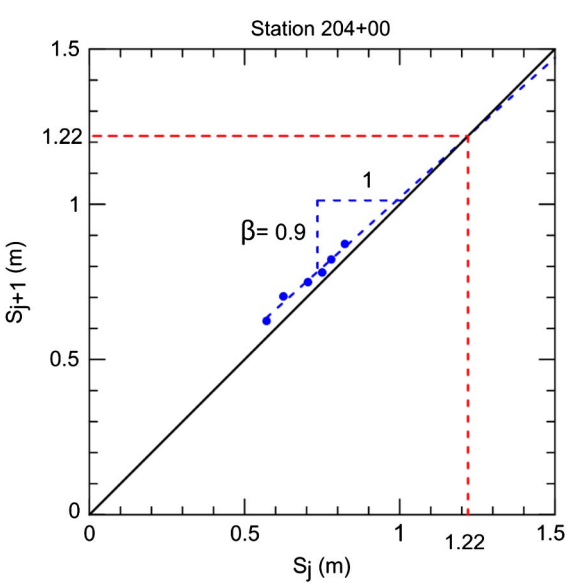

Fig. 8. Asaoka (1978) graphical method using settlements at different times for Station 204+00

During the initial subsurface investigation, one consolidation test was performed on a gray silt and clay specimen that exhibited liquid and plastic limits of 34 and 23, respectively. The results of this test yielded values of C_v of 1.78 and 2.47 m^2/year at effective stresses of 223 and 418 kPa, respectively (Table 3). Typically the ratio of C_h to C_v ranges from 1.5 to 4, so the range of C_h from the laboratory values of C_v presented previously is 2.7–9.9 m^2/year. This range of C_h is well below the design value of 18.6 m^2/year (200 ft^2/year).

Interestingly, the Asaoka (1978) method yielded a mobilized value of C_h of 6.4 m^2/year (68.6 ft^2/year) at Station 204+00, which yields a ratio of C_h to C_v of 3.6 to 2.6 using the laboratory consolidation test values of C_v of 1.78 and 2.47 m^2/year, respectively. In other words, the Asaoka (1978) method yielded a ratio of C_h to C_v of 2.6–3.6, which is in excellent agreement with the typical ratio of C_h to C_v of 1.5–4.0. In hindsight, a ratio of C_h to C_v of 1.5–4 could have been used with the laboratory values of C_v to develop a reasonable design range of C_h for the PVDs (2.7–9.9 m^2/year) instead of assuming a value of 18.6 m^2/year (200 ft^2/year).

The ratio of C_h to C_v of 1.5–4 also can be used to verify the design value of C_h using the laboratory values of C_v. For example, the design value of C_h of 18.6 m^2/year (200 ft^2/year) corresponds to a ratio of C_h to C_v of 10.4 and 7.5 using the laboratory values of C_v of 1.78 and 2.47 m^2/year, respectively. A range of C_h to C_v ratio of 10.4–7.5 is not within the typical range of 1.5–4, which should have been an indication that the design value of C_h was too optimistic and consolidation and undrained strength gain would not occur as fast as designed.

In summary, the value of C_h used for design of PVDs should be in agreement with the typical range of the ratio of C_h to C_v 1.5–4. The Asaoka (1978) method can be used to assess the mobilized value of C_h during filling and consolidation so that the fill process can be modified as needed to maintain embankment stability using the observational method described by Peck (1969).

Variances between estimated and mobilized values of C_h can result from soil type and the presence of a smear zone around the PVD, which is a cylinder of disturbed soil around the drain that is caused by the mandrel during PVD installation. The disturbed soil in the smear zone usually has a lower hydraulic conductivity and lower C_h than the soil outside the smear zone, which requires a longer time to reach the end of primary consolidation than that predicted. However, Mesri and Lo (1991) concluded that discharge capacity has a greater influence on degree of consolidation than does the radius of the soil cylinder and smear zone. Drains of poor quality or drains that are damaged during installation can slow consolidation more than the smear effect (Mesri and Lo 1991), so PVD discharge capacity should be maximized during PVD selection.

Degree of Consolidation

Fig. 9 shows the predicted increase in degree of consolidation with time for the C_h estimated using the Asaoka (1978) method at Station 204+00 (6.4 m^2/year) and the initial design of value of 18.6 m^2/year (200 ft^2/year). Failure of the Ramp ES embankment occurred approximately 1.5 months after placement of the embankment fill began, which corresponds to approximately 86% consolidation if C_h had been 18.6 m^2/year (200 ft^2/year) (Fig. 9). If C_h had been 18.6 m^2/year (200 ft^2/year), the undrained strength would have been sufficient to prevent embankment failure. However, using a time of 1.5 months and the mobilized value of C_h of

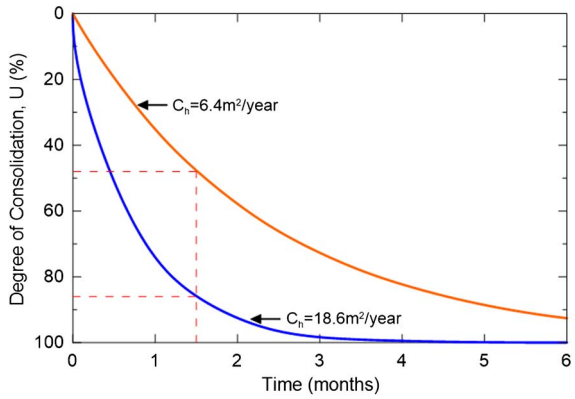

Fig. 9. Degree of consolidation versus time for Station 204+00 for the design and mobilized values of C_h

6.4 m^2/year (68.6 ft^2/year) from the Asaoka (1978) method at Station 204+00 yields a degree of consolidation of less than 50% consolidation, which helps explain the slope failure and low mobilized undrained shear strength of the foundation soils at the time of failure.

Evaluation of Slope Stability Analyses

Initial Analysis

The initial design analysis evaluated Ramp ES stability at a number of locations and fill phases using Bishop's modified stability method (Bishop 1955), as coded in the *PCSTABL6* software package. The six soil cross sections used in the initial analysis were developed using soil stratigraphy from the 24 borings completed along Ramp ES. Fig. 2 presents one of these six initial design cross sections, which was located at Station 201+61 and based on Boring ES-8A. This initial design cross section was the closest to the embankment failure area between Stations 202+00 and 205+00.

Foundation soil strengths were estimated using SPT N values and empirical correlations (Table 1) as described previously. The embankment fill strength parameters were estimated using procedures that are now outlined in GB-6 (ODOT 2010) but were not documented at the time of design. The ODOT specifications (ODOT 1995) require a minimum short-term or undrained factor of safety (FS) of 1.3 for embankment construction and a long-term or drained FS greater than 1.5. The initial FS values exceeded the minimum drained FS of 1.5 for all six initial design cross sections. However, four of the initial six design cross sections exhibited an undrained FS less than 1.3, which did not meet ODOT design requirements. One of these cross sections was based on Boring ES-8A near Station 201+61 (Fig. 2).

These four initial cross sections were reanalyzed by the designer with a flatter (2.5:1 horizontal:vertical instead of 2:1) slope, but the undrained FS did not increase significantly and all four cross sections still exhibited an undrained FS less than 1.3. These four cross sections were reanalyzed to determine a maximum staged embankment construction height that would yield an undrained FS greater than 1.3. The maximum slope height for each stage that would produce a minimum undrained FS of 1.3 was 4.6 m (15 ft) for the cross section based on Boring ES-8A. As a result, designers initially considered staged construction in increments of 4.6 m (15 ft) with sufficient time between stages to allow 90% consolidation of the foundation soils to occur. Later, the designers opted to construct the embankment slowly and continuously with pore-water pressure measurements and other monitoring instead of stopping fill placement after 4.6 m (15 ft). Neither of these design scenarios explain why the slope failure occurred at a fill height of only 4.0 m (13 ft), which is below the proposed staged increment of 4.6 m (15 ft), or why tension cracks started developing at a fill height of only 2.4 m (8 ft).

Postfailure Analysis

Although tension cracks developed from Stations 202+00 to 205+00 along Ramp ES, the actual slope failure was observed at Station 204+00, where movement of the right-of-way fence occurred (Fig. 7). To conduct an inverse analysis of the slope failure, a cross section was developed for Station 204+00 (Fig. 3) using Boring ES-8C, which was located nearby at Station 203+58. The cross section at Station 204+00 was analyzed herein using the Morgenstern and Price (1965) stability method included in the software package *SLOPE/W* developed by Geo-Slope and the results were compared with the original design analysis performed using the cross section based on Boring ES-8A (Fig. 2). Comparing the cross sections at Station 201+61 based on Boring ES-8A (Fig. 2) and Station 204+00 based on Boring ES-8C (Fig. 3) revealed the following important differences in the cross sections:

- There was a thicker (~6.1 m thick) weak soil layer ($S_u \leq 12$ kPa) at Station 203+58 than at Station 201+16 (~4.4 m thick);
- The weakest layer encountered along Ramp ES was located at Station 203+58 (S_u of 9.6 and 12 kPa), not at Station 201+16 ($S_u \geq 12$ kPa);
- The weakest layer at Station 203+58 was deeper (elevation 296.9–290.8 m) than at Station 201+16 (elevation 299.0–295.4 m), with the ground surface being approximately elevation 300.8 m; and
- There were different classifications for the weak soil layers between the two borings, e.g., peat and very soft clay at Station 203+58 and soft to medium clay at Station 201+16.

Compacted Fill Shear Strength

The shear strength of the compacted fill was reevaluated using guidance from GB-6 (ODOT 2010), which recommends an effective stress cohesion and friction angle of 14.4–26.3 kPa (400–550 psf) and 28–33° for the long-term strength of a compacted fill embankment. It is recommended that the effective stress friction angle (ϕ') be derived using the plasticity index and Eq. (10), which is included in GB-6. The average plasticity index of the fill material used for Ramp ES was approximately 10, based upon the design geotechnical report. Using a PI of 10 and Eq. (10), the estimated value of ϕ' is approximately 33°

$$\phi' = \frac{23.53(\mathrm{PI}) + 100.15}{\mathrm{PI}} \tag{10}$$

Using the failure surface estimated from field observations, e.g., tension cracks, displaced fence, scarp, slope inclinometer, and so on (Fig. 3), the inverse stability analysis performed herein estimated that an effective stress cohesion (c') of 14.4 kPa (300 psf) is required with a ϕ' of 33° to produce a FS of approximately 1.0 at a fill height of 4.0 m (13 ft), i.e., the failure height. This inverse analysis was used to estimate the mobilized c', because the value of ϕ' was estimated using Eq. (10) and has little influence on the calculated FS due to the failure surface being nearly vertical through the embankment (Duncan and Stark 1992) and the low normal stresses acting on the failure surface through the embankment

J. Geotech. Geoenviron. Eng., 2018, 144(2): 05017007

(Fig. 3). The strength parameters for the inverse stability analysis ($c' = 14.4$ kPa and $\phi' = 33$) were significantly lower than those used in the initial design analysis, which modeled the compacted fill with a total stress cohesion (c) or undrained shear strength of 71.8 kPa (1,500 psf) and a total stress friction angle (ϕ) of zero. This is in accordance with GB-6, which recommends using values of c of 71.8–95.8 kPa (1,500–2,000 psf) and ϕ of zero for the short-term analyses. The calculated FS using a c of 71.8 kPa (1,500 psf) and a fill height of 4.6 m (15 ft) was 1.64, which confirms that the original design met ODOT FS requirements but overpredicted the field FS because the slope failed, i.e., FS ~ 1.0.

Effect of Strength Parameters on Calculated Factor of Safety

Consistent with GB-6, the designers used a total stress cohesion and friction angle of zero to model the compacted fill embankment. However, values of cohesion can greatly influence the FS as illustrated using Bishop's stability method (Bishop 1955

$$\mathrm{FS} = \frac{\sum\left\{\frac{c+[(\frac{w}{b})-u]\tan(\phi)}{\psi}\right\}}{\sum\left[\frac{w}{b}\sin(\alpha)\right]} \tag{11}$$

where $\psi = \cos(\alpha) + [\sin(\alpha)\tan(\phi)]/\mathrm{FS}$; b = width of each slice; W = weight of each slice; u = pore-water pressure at the base of each slice; and α = orientation of the normal force with respect to horizontal. Using a ϕ of zero for the compacted fill as suggested in GB-6, this FS equation simplifies to

$$\mathrm{FS} = \frac{\sum\left[\frac{c}{\cos(\alpha)}\right]}{\sum\left[\frac{w}{b}\sin(\alpha)\right]} \tag{12}$$

The simplified equation leaves only the cohesion and orientation of the normal force (α) as the factors influencing the available resistance in the numerator. Because values of $\cos(\alpha)$ are small at the top of the failure surface, the resisting force in the fill material increases as cohesion increases. As a result, modeling shear strength of the compacted fill with only a cohesion value can overestimate the stability of a compacted fill slope on soft soils unless a tension crack is included in the analysis. For example, the FS for the initial embankment design was approximately 1.0 with a cohesion of 10 kPa (209 psf), but the FS increased to approximately 2.0 with a cohesion of 100 kPa (2,090 psf), ten times higher than 10 kPa (209 psf). For comparison, the initial design analysis modeled the compacted fill with $c = 71.8$ kPa (1,500 psf) and $\phi = 0$ and the calculated FS was 1.64, which is between unity and 2.0. In summary, if a compacted embankment is modeled with an undrained shear strength, a tension crack should be included in the stability analysis using the equation in the following section; otherwise the cohesion term will result in a large FS.

In this case, the unsaturated fine-grained compacted fill in the short-term or during construction slope stability analysis was also modeled using a ϕ' in the range of 28–35°, depending on plasticity [Eq. (10)], and c' of zero. This approach also yielded a factor of safety of approximately 1, which may have been fortuitous for this case history. In practice, it is prudent to evaluate stability using both undrained and drained strengths for the embankment to ensure stability for the short-term and long-term conditions, respectively.

Tension Crack

If an undrained shear strength is used to model a stiff compacted fill over soft foundation soils, a tension crack should be included in the embankment. A tension crack is required because of the strain incompatibility of the stiff embankment and the soft foundation soils. This results in the percentage of strength mobilized in the embankment being smaller than in the foundation soils (Chirapuntu and Duncan 1976). This incompatibility results in the tensile stresses developing in the embankment due to the lateral deformation of the soft foundation soils. This results in the development of a tension crack in the embankment. The depth of this tension crack, H_{crack}, can be estimated assuming a planar failure surface and force equilibrium using the following expression:

$$H_{\mathrm{crack}} = \frac{2c_{\mathrm{fill}}}{\gamma\mathrm{fill}\,\tan\left(45^0 - \frac{\phi_{\mathrm{fill}}}{2}\right)} \tag{13}$$

where γfill, ϕ_{fill}, and c_{fill} = unit weight, total stress friction angle, and total stress cohesion, respectively, of the compacted fill. For an undrained condition, the value of ϕ_{fill} is set to zero, so Eq. (13) reduces to

$$H_{\mathrm{crack}} = \frac{2c_{\mathrm{fill}}}{\gamma\mathrm{fill}} \tag{14}$$

Eq. (14) and a value of c_{fill} of 71.8 kPa (1,500 psf) results in a tension crack depth of 6.7 m [Eq. (15)]. Eq. (14) and a value of c_{fill} of 95.8 kPa (2,000 psf) results in a tension crack depth of 9.0 m [Eq. (16)]. Both of these crack depths correspond to the range of c_{fill} obtained from GB-6 and exceed the height of the embankment when the Ramp ES slope failure started at a fill height of 4.0 m (13 ft). As a result, no shear resistance should have been used for the embankment in the design stability analyses for Ramp ES because an undrained shear strength was being used to model the compacted fill strength

$$H_{\mathrm{crack}} = \frac{2c_{\mathrm{fill}}}{\gamma\mathrm{fill}} = \frac{2(71.8\ \mathrm{kPa})}{21.2\,\frac{\mathrm{kN}}{\mathrm{m}^3}} = 6.7\ \mathrm{m} \tag{15}$$

$$H_{\mathrm{crack}} = \frac{2c_{\mathrm{fill}}}{\gamma\mathrm{fill}} = \frac{2(95.8\ \mathrm{kPa})}{21.2\,\frac{\mathrm{kN}}{\mathrm{m}^3}} = 9.0\ \mathrm{m} \tag{16}$$

For the initial design cross section at Station 201+61 based on Boring ES-8A (Fig. 2), the critical factor of safety using a circular failure surface search, shear strengths shown in Fig. 2, no tension crack, and one-half of the final embankment height or 4.6 m (15 ft) is 1.59, which indicates stability. However, this limit equilibrium analysis showed significant tension in the upper portion of the embankment, i.e., negative normal stresses on the base of several of the vertical slices in the embankment.

Performing the same analysis with a tension crack for the full embankment depth, i.e., 4.6 m (15 ft) as suggested by Eq. (14), yields a critical factor of safety of 0.91. Therefore if an appropriate tension crack had been included in the initial design stability analysis, failure would have been predicted. The embankment failed at a height of only 4.0 m (13 ft), so the same analysis was performed with a tension crack the full height of the constructed embankment, i.e., 4.0 m (13 ft), and the critical factor of safety was 1.02, which is in excellent agreement with the slope failure occurring at an embankment height of 4.0 m (13 ft).

For the postfailure cross section at Station 203+58 based on Boring ES-8C (Fig. 3), the critical factor of safety using a circular search, the shear strengths in Fig. 3, no tension crack, and an embankment height of 4.0 m (13 ft) is 1.44, which also indicates stability, but this factor of safety is less than the 1.59 calculated for Station 201+61. Performing the same analysis with a tension crack, the full embankment depth, i.e., 4.0 m (13 ft), yielded a critical circular factor of safety of 1.06, which also is in agreement with the slope failure. Because this factor of safety is above unity, the same analysis with a tension crack the full embankment depth, i.e., 4.0 m (13 ft), and a noncircular failure surface was also conducted, and the critical factor of safety was 0.98, which is in better agreement with the slope failure occurring at 4.0 m (13 ft). In summary, the embankment fill did not mobilize significant shear resistance to improve the overall factor of safety due to strain incompatibility and tensile stresses and cracking developing in the fill, which contributed to the slope failure.

The development of tensile stresses and cracking in compacted embankments founded on soft clay foundations described previously is reinforced by the numerical analyses presented by Chirapuntu and Duncan (1976). These finite element analyses show that when an embankment is significantly stronger and stiffer that the underlying foundation soils, the percentage of strength mobilized in the embankment is smaller than in the foundation (Chirapuntu and Duncan 1976). In particular, the greater the disparity between the embankment and foundation strengths, the lower the mobilized shear resistance in the compacted embankment. Chirapuntu and Duncan (1976) also showed that tension develops in the embankment due to the soft foundation soils squeezing from beneath the embankment centerline to the slope toe causing cracks to propagate from the bottom to the top of the embankment. Chirapuntu and Duncan (1976) presented the following expression for estimating the depth of the tension crack that will develop in a compacted embankment over a soft clay foundation:

$$H_{\text{crack}} = 5.1\left(\frac{c_{\text{foundation}}}{\gamma\text{fill}}\right)\left(\frac{K_{\text{foundation}}}{K_{\text{fill}}}\right)^{0.75}\left(\frac{W}{D}\right)^{0.25} =$$

$$H_{\text{crack}} = 5.1\left(\frac{17.9\ \text{kPa}}{21.2\frac{\text{kN}}{\text{m}^3}}\right)\left(\frac{120}{150}\right)^{0.75}\left(\frac{27.6\ \text{m}}{8.5\ \text{m}}\right)^{0.25} = 4.9\ \text{m} \quad (17)$$

where $c_{\text{foundation}}$ = average foundation undrained shear strength, which was 17.9 kPa at Station 203+58 (Fig. 3) in the failed area, as calculated subsequently; $K_{\text{foundation}}$ = foundation modulus number, which was estimated to range from 40 to 150 using PI < 30, average $c_{\text{foundation}}$ of 17.9 kPa, and a correlation in Chirapuntu and Duncan (1976); K_{fill} = embankment fill modulus number, which was estimated to range from 150 to 600 using a soil type SC, an optimum water content, and data in Chirapuntu and Duncan (1976); γfill = embankment fill unit weight, which was 21.2 kN/m^3 (135 pcf); W = width of Ramp ES embankment, which was 27.6 m with a crest width of 11.6 m; and D = depth of the soft foundation soils, which was 8.5 m (Fig. 3).

The empirical relationship developed by Chirapuntu and Duncan (1976) in Eq. (17) yields a tension crack depth of only 4.9 m, which is less than the value of 6.7 m estimated using Eq. (15). The numerical analyses performed by Chirapuntu and Duncan (1976) probably resulted in a better representation of the strain incompatibility between the stiff embankment and soft foundation soils, and thus a smaller tension crack depth, than the force equilibrium expression in Eq. (15). Regardless, a tension crack depth of 4.9 m still exceeds the height of the embankment when the slope failed at 4.0 m (13 ft) and also suggests that the embankment fill did not mobilize significant shear resistance to improve the overall factor of safety. Therefore the empirical expression developed by Chirapuntu and Duncan (1976) also accurately predicts the Ramp ES slope failure and can be used in future design to predict tension crack depth.

Long-Term Embankment Shear Strength

In a long-term or drained slope stability analysis, the fine-grained compacted fill material should be modeled using a stress-dependent strength envelope as suggested by Stark and Hussain (2013) that corresponds to the drained fully softened strength (FSS) to conservatively estimate the long-term stability, i.e., after long-term wet-dry cycles, infiltration, swelling, and softening. The peak strength of compacted specimens should not be used because the effects of compaction can be reduced by wet-dry cycles as detailed by Kayyal and Wright (1991), Saleh and Wright (1997), and Wright et al. (2007). Stark and Hussain (2013) and Gamez and Stark (2014) presented stress-dependent empirical correlations for drained FSS strengths based on liquid limit and clay-size fraction that have been validated via case histories and laboratory testing.

FS Verification and Allowable Fill Height

Even though design limit equilibrium stability analyses may indicate an adequate FS, e.g., 1.64 using $c = 71.8$ kPa (1,500 psf) and the initial staged fill height of 4.6 m (15 ft) in this project, the value of FS or allowable fill height should be verified. The FS, or allowable fill height, can be easily estimated using an undrained bearing capacity analysis, as discussed subsequently, before stability analyses are conducted to help guide the embankment design. An undrained bearing capacity analysis can be solved for the FS or allowable height of fill for a given FS as suggested by Peck et al. (1974) and included in Homework Problem #10 on Page 303 of Peck et al. (1974). Professor Stephen G. Wright also mentioned the use of an undrained bearing capacity analysis to estimate the embankment FS in his 2013 H. Bolton Seed Lecture (Wright 2013). This analysis is accomplished using a weighted average value of S_u ($S_{u,\text{avg}}$) along a failure surface, a bearing capacity factor, N_c, of 5.14, the desired fill height (H_{fill}), and unit weight of the compacted fill (γfill)

$$\text{FS} = \frac{N_c S_{u,\text{avg}}}{\gamma\text{fill}\, H_{\text{fill}}} \quad (18)$$

A value of N_c equal to 5.14 is used because the depth of embedment of the embankment is zero and the embankment is modeled as a strip footing. For the failed subsurface cross section at Station 203+58 based on Boring ES-8C (Fig. 3), the weighted value of $S_{u,\text{avg}}$ can be estimated using a weighted average based on the length of the failure surface in each layer. This is a reasonable estimate of $S_{u,\text{avg}}$ when S_u is measured using unconsolidated-undrained (UU) triaxial compression tests because the specimens have some disturbance, which counter-balances the different modes of shear present along the failure surface. As a result, a value of $S_{u,\text{avg}}$ based on UU triaxial compression tests represents the mobilized S_u derived from triaxial compression, direct simple shear, and triaxial extension modes of shear present along the failure surface in Fig. 3. The weighted value of $S_{u,\text{avg}}$ is calculated as follows:

J. Geotech. Geoenviron. Eng., 2018, 144(2): 05017007

$$S_{u,\text{avg}} = \frac{36\ \text{kPa}(2.4\ \text{m}) + 12\ \text{kPa}(1.5\ \text{m}) + 12\ \text{kPa}(1.6\ \text{m}) + 9.6\ \text{kPa}(3.0\ \text{m})}{(2.4\ \text{m} + 1.5\ \text{m} + 1.6\ \text{m} + 3.0\ \text{m})}$$
$$S_{u,\text{avg}} = \frac{86.4\ \text{kPa}\cdot\text{m} + 18.0\ \text{kPa}\cdot\text{m} + 19.2\ \text{kPa}\cdot\text{m} + 28.8\ \text{kPa}\cdot\text{m}}{8.5\ \text{m}} =$$
$$S_{u,\text{avg}} = \frac{152.4\ \text{kPa}\cdot\text{m}}{8.5\ \text{m}} = 17.9\ \text{kPa} \tag{19}$$

On August 1, 2007, the embankment reached a height of 4.0 m (13 ft), with an average unit weight of 21.2 kN/m^3 (135 pcf) (Table 7), which corresponds to an increase in total stress of 84.8 kPa. The resulting FS using the simplified bearing capacity expression is 1.08 [Eq. (20)], which is in agreement with the onset of failure on August 1, 2007:

$$\text{FS} = \frac{N_c S_{u,\text{avg}}}{\gamma\text{fill}\, H_{\text{fill}}} = \frac{5.1417.9\ \text{kPa}}{21.2\frac{\text{kN}}{\text{m}^3}\times 4.0\ \text{m}} = 1.08 \tag{20}$$

The overall degree of consolidation in Fig. 9 is approximately 45%, so the strength gain due to the fill height at the centerline can be estimated to refine the bearing capacity analysis in Eq. (20). This is investigated even though the critical failure surface in Fig. 3 does not extend to the embankment centerline. Using a fill height of 4.0 m (13 ft) and a fill unit weight of 21.2 kN/m^3, an increase in total stress of 84.8 kPa was applied at the fill centerline. This corresponds to an increase in effective stress of 38.1 kPa for a 45% degree of consolidation. An increase of 38.1 kPa was multiplied by the mobilized S_u/σ'_p ratio of 0.22 to estimate the increase in undrained shear strength of 8.4 kPa at the embankment centerline. For the failed subsurface cross section at Station 203+58 based on Boring ES-8C (Fig. 3), the value of $S_{u,\text{avg}}$ can be estimated using the length of the failure surface in each layer and assuming the undrained strength increased by 8.4 kPa at the embankment centerline in the upper layer, i.e., A-6b soil layer, due to stress distribution with depth. The total settlement on August 1, 2007 was only 0.48 m so it is assumed that most of the observed settlement occurred in the upper layer because of its thickness and close proximity to the overlying fill. The value of $S_{u,\text{avg}}$ after 45% consolidation is termed $S_{u,\text{consol-avg}}$ and is calculated as follows:

$$S_{u,\text{consol-avg}} = \frac{(36 + 8.1\ \text{kPa})(2.4\ \text{m}) + (12\ \text{kPa})(1.5\ \text{m}) + (12\ \text{kPa})(1.6\ \text{m}) + 9.6\ \text{kPa}(3.0\ \text{m})}{(2.4\ \text{m} + 1.5\ \text{m} + 1.6\ \text{m} + 3.0\ \text{m})}$$
$$S_{u,\text{consol-avg}} = \frac{105.8\ \text{kPa}\cdot\text{m} + 18.0\ \text{kPa}\cdot\text{m} + 19.2\ \text{kPa}\cdot\text{m} + 28.8\ \text{kPa}\cdot\text{m}}{8.5\ \text{m}} =$$
$$S_{u,\text{consol-avg}} = \frac{171.8\ \text{kPa}\cdot\text{m}}{8.5\ \text{m}} = 20.2\ \text{kPa} \tag{21}$$

The resulting FS using the simplified bearing capacity expression is 1.22 [Eq. (22)], which is not in agreement with the onset of failure on August 1, 2007. Therefore the predicted increase in $S_{u,\text{avg}}$ for a degree of consolidation of 45% under a fill height of 4.0 m (13 ft) is probably too high, but the calculation still shows that the embankment does not meet the design value of FS of 1.3

$$\text{FS} = \frac{N_c S_{u,\text{consol-avg}}}{\gamma\text{fill}H_{\text{fill}}} = \frac{5.14(20.2\ \text{kPa})}{21.2\frac{\text{kN}}{\text{m}^3}(4.0\ \text{m})} = 1.22 \tag{22}$$

The expression in Eq. (20) can be used to estimate the FS for other embankment heights and the subsurface cross-section at Station 203+58 based on Boring ES-8C (Fig. 3). Table 11 shows that a two-stage construction of the embankment using a fill height of 4.6 m (15 ft) would not be stable (FS = 0.94), nor would the full embankment height of 9.2 m (30 ft) at this location (FS = 0.47). This bearing capacity analysis also indicates that the embankment should have been stable (FS = 1.81) at a fill height of 2.4 m (8 ft) even though tension cracks were first observed at this height. The embankment did not fail until the fill height reached 4.0 m (13 ft), and it was stable from July 7, 2007 to August 1, 2007. As a result, the bearing capacity analysis evaluates the failure condition so tension cracks and slope movement can occur before the FS reaches unity. However, this simple analysis shows the sensitivity of the FS to fill height because increasing the fill height from 2.4 (8 ft) to 4.0 m (13 ft) decreased the FS from 1.81 to 0.94. Performing this simple analysis before starting the limit equilibrium stability analyses can help the practitioner see the forest from the trees and guide the detailed embankment design.

The expression in Eq. (18) also can be rearranged to estimate the allowable fill height for a given FS, e.g., FS = 1 as shown Eq. (23), to obtain a quick estimate of a maximum allowable embankment height

$$H_{\text{fill}} = \frac{N_c S_{u,\text{avg}}}{\gamma\text{fill}\text{FS}} = \frac{5.14\times 17.9\ \text{kPa}}{21.2\frac{\text{kN}}{\text{m}^3}\times 1.0} = 4.3\ \text{m} \tag{23}$$

Different values of FS can be used in Eq. (23), but this calculation shows that the allowable fill height is only 4.3 m for FS = 1, and on August 1, 2007 the fill height was 4.0 m, which is in agreement with the onset of embankment failure.

J. Geotech. Geoenviron. Eng., 2018, 144(2): 05017007

Table 11. Bearing Capacity Values of FS for Different Embankment Heights for the Subsurface Cross-Section at Station 203+58 Based on Boring ES-8C (Fig. 3)

Embankment fill condition	Embankment height (H_{fill}) [m (ft)]	Bearing capacity FS using Eq. (20)
July 7, 2007—tension cracks first observed	2.4 (8)	1.81
August 1, 2007—tension cracks restart	4.0 (13)	1.08
Stage 1 fill height	4.6 (15)	0.94
Full embankment height	9.2 (30)	0.47

Summary and Recommendations

Based on the postfailure PVD and slope stability analyses performed for Ramp ES, the following recommendations are made for evaluating the stability of stiff, compacted embankments over soft foundation soils:

- If the stiff, compacted embankment overlying soft foundation soils is modeled with an undrained shear strength and a friction angle of zero, a tension crack must be included in the stability analysis; otherwise, the strength of the embankment will be overestimated. The depth of the tension crack can be estimated using force equilibrium and a planar failure surface derived expression in Eq. (13) or the empirical expression developed by Chirapuntu and Duncan (1976) in Eq. (17).
- If undrained strength data are not available for the weak foundation soils, index properties, such as plasticity index, can be used to estimate an undrained strength ratio, which can be used to estimate undrained shear strength profiles using Eqs. (1)–(3) or simply using a mobilized undrained strength ratio of 0.22. These correlations are more reliable than SPT-based correlations for clays. Peck et al. (1974) stated that standard penetration correlations "for clays can be regarded as no more than a crude approximation, but that for sands is often reliable enough to permit the use of N-values in foundation design." As a result, cone penetration tests are a better option for estimating the shear strength of clays than are SPTs (Terzaghi et al. 1996; Jamiolkowski et al. 1985; Holtz and Kovacs 1981).
- Cross sections for stability analyses of a long embankment can be selected based on changes in soil stratigraphy and shear strength. It is recommended that attention be given to locations that exhibit a large change in undrained shear strength and depth to the weakest foundation soil layer because these factors influence the depth of the tension crack and undrained factor of safety.
- An undrained bearing capacity factor of safety can be useful for guiding limit equilibrium slope stability analyses for a compacted embankment over soft foundation soils and estimating a reasonable allowable embankment height to guide the design.
- For a long-term slope stability analysis, a stress-dependent fully softened strength envelope passing through the origin should be used to account for the impact of wet/dry cycles, infiltration, swelling, and softening of the shear strength of compacted fill with time (Stark and Hussain 2013).
- A reasonable range of the ratio of horizontal to vertical coefficient of consolidation is 1.5–4.0. This empirical range can be used to guide selection of the initial value of the horizontal coefficient of consolidation for PVD design instead of estimating a value or it can be used to confirm laboratory data.
- The Asaoka (1978) method can be used during embankment construction and settlement to estimate the mobilized value of horizontal coefficient of consolidation for comparison with the design value to verify that consolidation and strength gain are occurring as predicted. If consolidation is not occurring as fast as predicted, then fill placement can be modified to maintain stability, which is in agreement with the observational method proposed by Peck (1969).

Acknowledgments

The contents and views in this paper are those of the individual authors and do not necessarily reflect those of any of the represented corporations, contractors, agencies, consultants, organizations, and/or contributors, including ODOT. The authors also gratefully acknowledge the extensive and beneficial comments of Reviewers 2 and 3, which greatly clarified and improved this case study.

Supplemental Data

Figs. S1 and S2, and Appendixes S1–S4 are available online in the ASCE Library (www.ascelibrary.org).

References

Asaoka, A. (1978). "Observational procedure of settlement prediction." *Soils Found. J. Jpn. Geotech. Soc.*, 18(4), 87–101.

ASTM. (2007). "Standard test method for particle-size analysis of soils." *ASTM D422/D422M-07*, West Conshohocken, PA.

ASTM. (2009). "Standard practice for description and identification of soils (visual-manual procedure)." *ASTM D2488-09*, West Conshohocken, PA.

ASTM. (2010a). "Standard test method for liquid limit, plastic limit, and plasticity index of soils." *ASTM D4318/D4318M-10*, West Conshohocken, PA.

ASTM. (2010b). "Standard test methods for laboratory determination of water (moisture) content of soil and rock by mass." *ASTM D2216-10*, West Conshohocken, PA.

ASTM. (2011a). "Standard test method for consolidated-undrained triaxial compression test for cohesive soils." *ASTM D4767-11*, West Conshohocken, PA.

ASTM. (2011b). "Standard test method for one-dimensional consolidation properties of soils using incremental loading." *ASTM D2435/D2435M-11*, West Conshohocken, PA.

ASTM. (2013a). "Standard classification of peat samples by laboratory testing." *ASTM D4427–13*, West Conshohocken, PA.

ASTM. (2013b). "Standard test method for unconfined compressive strength of cohesive soils." *ASTM D2166/2166M-13*, West Conshohocken, PA.

ASTM. (2014a). "Standard test method for moisture, ash, and organic matter of peat and other organic soils." *ASTM D2974-14*, West Conshohocken, PA.

ASTM. (2014b). "Standard test method for specific gravity of soli solids by water pycnometer." *ASTM D854-14*, West Conshohocken, PA.

Bishop, A. W. (1955). "The use of slip circles in the stability analysis of earth slopes." *Geotechnique*, 5(1), 7–17.

Bowles, J. E. (1977). *Foundation analysis and design*, 1st Ed., McGraw-Hill, New York.

Bowles, J. E. (1996). *Foundation analysis and design*, 5th Ed., McGraw-Hill, New York.

Chirapuntu, S., and Duncan, J. M. (1976). "The role of fill strength in the stability of embankments on soft clay foundations." *Rep. No. TE-75-3*, U.S. Army Engineer, Waterways Experiment Station, Washington, DC.

Duncan, J. M., and Stark, T. D. (1992). "Soil strengths from back-analysis of slope failures." *Proc., Specialty Conf. Stability and Performance of Slopes and Embankments-II*, Vol. 1, ASCE, Berkeley, CA, 890–904.

Gamez, J., and Stark, T. D. (2014). "Fully softened shear strength at low stresses for levee and embankment design." *J. Geotech. Geoenviron. Eng.*, 10.1061/(ASCE)GT.1943-5606.0001151, 06014010-1–06014010-6.

Holtz, R. D., and Kovacs, W. D. (1981). *An introduction to geotechnical engineering*, Prentice-Hall, Englewood Cliffs, NJ, 733.

Holtz, R. D., Kovacs, W. D., and Sheahan, T. C. (2011). *An introduction to geotechnical engineering*, Prentice-Hall, Englewood Cliffs, NJ, 653.

Jamiolkowski, M., Ladd, C. C., Germaine, J. T., and Lancellotta, R. (1985). "New developments in field and laboratory testing of soils." *Proc., 11th Int. Conf. on Soil Mechanics and Geotechnical Engineering*, Vol. 1, A.A. Balkema, Rotterdam, Netherlands, 57–153.

Kayyal, M. K., and Wright, S. G. (1991). "Investigation of long-term strength properties of Paris and Beaumont clays in earth embankments." *Research Project No.CTR 3-8-89/1-1195-2F, Research Rep. 1195-2F*, Center for Transportation Research, Univ. of Texas, Austin, TX.

Lo, D. O. K. (1991). "Soil improvement by vertical drains." Ph.D. thesis, Univ. of Illinois at Urbana-Champaign, Champaign, IL.

Mesri, G., and Huvaj, N. (2009). "The Asaoka method revisited." *Proc., 17th Int. Conf. in Soil Mechanics and Geotechnical Engineering*, Vol. 1, IsoPress, Amsterdam, Netherlands, 131–134.

Mesri, G., and Lo, D. O. K. (1991). "Field performance of prefabricated vertical drains." *Proc., Int. Conf. on Geotechnical Engineering For Coastal Development—Theory to Practice*, Vol. 1, Coastal Development Institute of Technology, Tokyo, 231–236.

Morgenstern, N. R., and Price, V. E. (1965). "The analysis of the stability of general slip surface." *Geotechnique*, 15(1), 79–93.

ODOT (Ohio Department of Transportation). (1995). *Construction and material specifications*, Columbus, OH.

ODOT (Ohio Department of Transportation). (2010). *GB-6: Geotechnical Bulletin No. 6—Shear strength of proposed embankments*, Division of Production Management Office of Geotechnical Engineering, Columbus, OH, 7.

PCSTABL6 [Computer software]. Dept. of Civil Engineering, Purdue Univ., West Lafayette, IN.

Peck, R. B. (1969). "Advantages and limitations of the observational method in applied soil mechanics." *Geotechnique*, 19(2), 171–187.

Peck, R. B., Hanson, W. E., and Thornburn, T. H. (1974). *Foundation engineering practice*, 3rd Ed., Wiley, New York, 514.

Saleh, A. A., and Wright, S. G. (1997). *Shear strength correlations and remedial measure guidelines for long-term stability of slopes constructed of highly plastic clay soils*, Center for Transportation Research, Univ. of Texas, Austin, TX, 156.

Slope/W [Computer software]. Geo-Slope International, Calgary, Canada.

Stark, T. D., and Hussain, M. (2013). "Drained shear strength correlations for slope stability analyses." *J. Geotech. Geoenviron. Eng.*, 10.1061/(ASCE)GT.1943-5606.0000824, 853–862.

Terzaghi, K., Peck, R. B., and Mesri, G. (1996). *Soil mechanics in engineering practice*, 3rd Ed., Wiley, New York, 549.

Urzua, A., Ladd, C. C., and Christian, J. T. (2016). "New approach to analysis of consolidation data at early times." *J. Geotech. Geoenviron. Eng.*, 10.1061/(ASCE)GT.1943-5606.0001523, 06016009-1–06016009-6.

Wright, S. G. (2013). "Slope stability computations." ⟨https://www.youtube.com/watch?v=Q_6aOU7msBM⟩ (Mar. 3, 2013).

Wright, S. G., Zornberg, J. G., and Aguettant, J. E. (2007). *The fully softened shear strength of high plasticity clays*, Center for Transportation Research, Univ. of Texas, Austin, TX, 132.